International Journal of Remote Sensing
Vol. 26, No. 19, 10 October 2005, 4321–4337

Results from the EO-1 experiment—A comparative study of Earth Observing-1 Advanced Land Imager (ALI) and Landsat ETM+ data for land cover mapping in the Okavango Delta, Botswana

AMY L. NEUENSCHWANDER*†, MELBA M. CRAWFORD† and SUSAN RINGROSE‡

†Center for Space Research, University of Texas at Austin, 3925 W. Braker Lane, Suite 200, Austin, TX 78759-5321, USA
‡Harry Oppenheimer Okavango Research Centre, University of Botswana, Private Bag 285, Maun, Botswana

The Earth Observing-1 (EO-1) satellite acquired a sequence of data in 2001 and 2002 that highlighted the annual flooding of the lower Okavango Delta. The data were collected as part of the calibration/validation programme for the Advanced Land Imager (ALI) sensor on the NASA EO-1 satellite. The primary purpose of this study was to compare the capability of ALI to that of Landsat ETM+ for large-scale mapping applications in the Okavango Delta. While the extent and inaccessibility of many areas of the Delta make application of remote sensing attractive, the availability of data with adequate spatial and spectral resolution has limited the characterization of the complex patterns of land cover and geomorphology in the Delta. Initial analysis of the ALI data via supervised classification clearly showed macro-flood features, delineation of downstream channel flow areas, and lateral-downstream inundation of the floodplain. These patterns and the proportions of flooding of the channel compared to that of the floodplain (impoundment) varied annually, from the wetter seasonal swamps through the drier seasonal and occasional swamps. Consistently higher classification accuracies achieved using ALI data relative to ETM+ data are attributed to the higher signal-to-noise ratio and the increased dynamic range of the ALI data.

1. Introduction

Wetland ecosystem processes comprise a critical element of Earth system science, since they are rich in productivity and species biodiversity (flora and fauna); they function as water storage and pollution buffering systems; and they often provide resources for livelihood to local communities and villages (Keddy 2000). The Okavango Delta in northern Botswana is one of the world's largest freshwater wetlands (~20 000 km^2). The region is typified by a semi-arid climatic regime with an annual average rainfall in Maun of 460 mm. Much of the rainfall is localized during the rainy season, with extended periods of drought during the dry months. Here, flooding occurs during the winter dry season (June through August) due to rainfall runoff from the Angolan highlands. Much of the vegetation is dormant

*Corresponding author. Email: amy@csr.utexas.edu

during the winter season, so vegetational response is essentially in the form of regeneration.

The assessment of flood responses in wetlands may be tenuous, particularly in such areas as the Okavango, as hydrologic sub-environmental adaptive factors differ, thereby contributing to unique ecosystem development (Ringrose *et al*. in press b). Much of the Okavango Delta, a relatively protected wetland under the Ramsar Convention, falls within the Zambesian regional centre of endemism (White 1983) and comprises extensive floodplains that may be permanently, seasonally, occasionally, or rarely wet (MLGLH 1989). At local scales, the response of vegetation along floodplains is characterized by heterogeneity due to hydrological, edaphic and land-use factors (McCarthy and Ellery 1993, McCarthy *et al*. 1997, Ringrose *et al*. 1997). Varying degrees of disturbance (e.g. elephant impacts) and local climatic factors are also important (Wolski *et al*. 2002). Previous work provides evidence that much of the ~97% water loss from the Okavango can be attributed to high rates of evapotranspiration (1000–1500 mm $year^{-1}$), thereby resulting in characteristic geochemical precipitates (within clastic sediments) (McCarthy *et al*. 1998). However, these theories have not yet been tested on a large spatial scale due to the expanse and general inaccessibility of the Delta.

Much of the Delta is a designated wildlife preserve, and tourism is limited. Further, roads are impassable during both the summer rainy season and winter flooding, thereby making field-based studies difficult to conduct. Thus, remote sensing provides a primary data source for deriving information about the vegetation and hydrologic regime of the area. Vegetation grows in patches, exhibits seasonal variation, and changes in response to subtle topographic variation on a scale of metres. Thus, medium-/high-resolution multispectral space-based data provide suitable sources for regularly monitoring flood events and associated vegetation responses. While results of previous Landsat Thematic Mapper based investigations (Ringrose *et al*. 1988, 1997, 2003, 2005) were promising, the increased dynamic range, improved signal-to-noise ratio, and additional multispectral bands provided by the Advanced Land Imager (ALI) instrument on the NASA Earth Observing-1 (EO-1) satellite potentially provide improved capability for characterizing the ecology of the Delta and mapping flood events. This includes tracking the progression of the flood toward the distal regions of the Delta and mapping and characterizing the response of floodplain vegetation before, during, and subsequent to inundation.

Specific aims of the research reported here were as follows:

- to investigate the contribution of additional bands in the ALI multispectral data for discriminating land cover compared to Landsat ETM+; and
- to investigate variability in annual flood patterns of the lower Okavango Delta during the EO-1 mission.

2. Study area

The EO-1 satellite acquired data over a study area centred on the Harry Oppenheimer Okavango Research Center (HOORC) field site located on Chief's Island (within Landsat ETM+ 174/74). This study area is approximately 2400 km^2 in size and is shown in figure 1. The vegetation in the study area is characterized by seasonal and occasional swamps as well as drier woodlands. Seasonally flooded

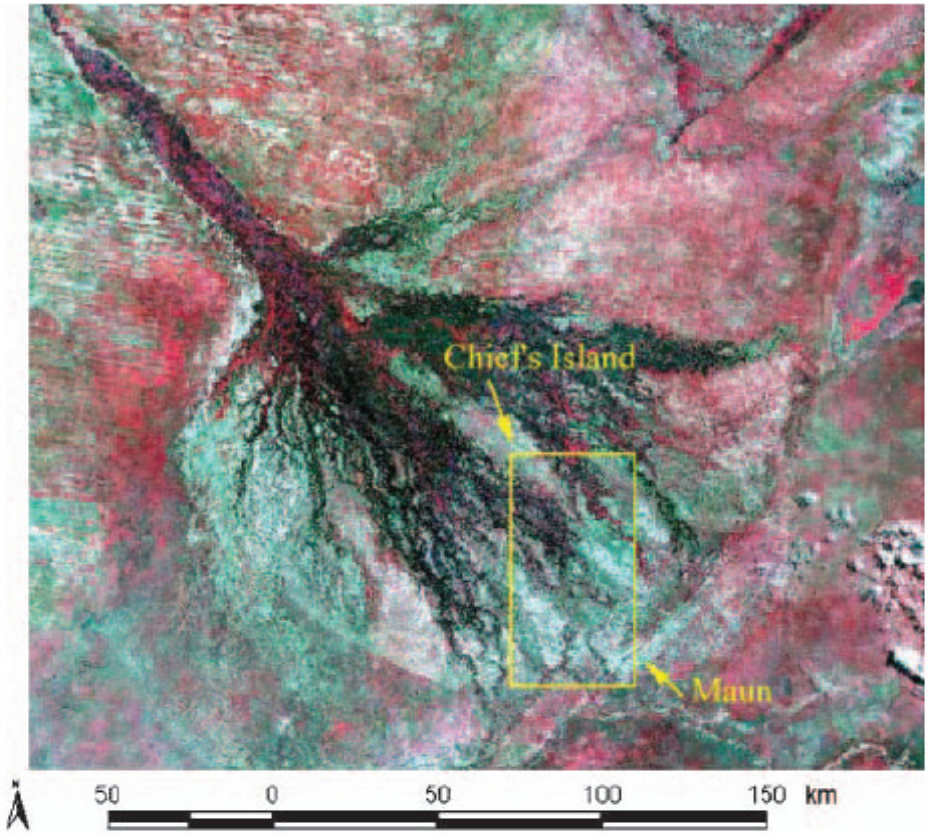

Figure 1. Map of Okavango Delta depicting the ETM+ and ALI study area.

grasslands (also known as seasonal swamps) cover the primary floodplain and flood annually. Occasional swamps flood at 1- to 10-year intervals and comprise primarily grasslands, but include some shrubs and other woodland species, as there is adequate time for these vegetation types to develop between flooding events.

The land cover classes in the study area (table 1) are modified after the Botswana Ministry of Local Government Lands and Housing ecological zonation for the Okavango Delta (MLGLH 1989). The floodplains of the seasonal swamps contain large stands of sedges including *Schoenoplectus corymbosus* and *Cyperus articulatus*. Also common in the seasonal swamps are reeds (*Phragmites communis*), bulrush (*Typha capensis*), and grass (*Miscanthus junceus*). The secondary floodplains within the seasonal swamps are typically covered by large grasslands that include species such as *Panicum repens*, *Sorgastrum friesii*, and *Imperata cylindrica*. The drier portions of the occasional swamps also contain dry grass species such as *Panicum repens*, *Andropogon*, and *Stripagrostis uniplumis*, as well as shrubs such as *Pechuel-loeschea leubnitziae*. The woodlands, typically dominated by *Colosphernum mopane, Combretum imberbe, Terminalia sericea*, and *Acacia* spp., are located on drier soils.

3. Data and methods

3.1 *Remotely sensed data*

The NASA Earth Observing-1 (EO-1) satellite was launched in November 2000 as a demonstration for several technologies, including the Advanced Land Imager (ALI) sensor, a multispectral pushbroom prototype for the Landsat Data Continuity Mission (LDCM). The EO-1 satellite orbits at 705 km altitude and follows

Table 1. Definition of land cover classes identified in ALI Imagery (modified after MLGLH 1989).

Ecosystem	Definition	Main species
North riparian zone	Linear fringe bordering islands and channels	*Ficus sycamorus, Acacia* spp., *Hyphaena petersiana*
South riparian zone	Linear fringe bordering islands and channels	*Combretum imberbe, Lochocarpus capassa, Croton megalobotryis*
Mopane shrublands	Stunted form of mopane on fine soils	*Colophospernum mopane*
Mopane woodlands	Monospecific close to wetland edges mixed in drier soils	*Colophospernum mopane*
Woodland mix	Mixed woodland species on drier soils	*C. mopane, Terminalia sericea Combretum imberbe*
Acacia mix woodlands	Sandier areas including former floodplains	*Acacia erioloba, Acacia tortillis, Terminalia sericea*
Acacia woodland on Chief's Island	Ecotone between riparian zone and *C. mopane* on edge of Chief's Island	*Acacia* spp.
Acacia shrubland on Chief's Island	Extensive areas of acacia, shrubs such as pechuel and grasses	*Acacia* spp., *Panicum* spp., *Pechuel-loeschea leubritziae Andropogon* spp.
Acacia grassland on Chief's Island	Extensive grasslands with less acacia and shrubs	*Acacia* spp., *Panicum* spp., *Pechuel-loeschea leubritziae, Andropogon* spp.
Grass, mopane, pechuel mixed shrublands	Extensive areas of dry grasses/shrubs with occasional mopane. Occurs on drier soils	*Colophospernum mopane, Pechuel-loeschea leubritziae, Panicum* spp., *Andropogon* spp.
Grass, pechuel mixed shrubland	Extensive areas of dry grasses/ shrubs	*Pechuel-loeschea leubritziae, Panicum* spp., *Andropogon* spp.
Island interior grasses	Infrequently flooded areas of higher salinity/alkalinity	*Cyperus laevigatus, Sporobolus spicatus*
Reeds	Frequently flooded grasses adjacent to channels	*Phragmites australis, Cyperus articulatus*
Backswamp	Frequently flooded grasses	*Cynadon doctylon, Hyparrheria* spp.
Floodplain grasses 1	Tall grasses seasonally inundated	*Cynadon doctylon, Hyparrheria* spp.
Floodplain grasses 2	Short grasses seasonally inundated	*Cynadon doctylon, Imperata cylindirica, Cymbopogon excavatus*
Floodplain grasses 3	Infrequently flooded extension of the occasional swamps	*Panicum* spp., *Andropogon* spp., *Aristidia* spp.
Aquatic vegetation	Mainly floating aquatic vegetation	*Vossia cuspidata, Miscanthus junceus*

approximately 1 min behind the Landsat 7 satellite in the (Landsat, EO-1, SAC-C, Terra) AM constellation (Ungar *et al.* 2003). Because the ALI was developed as a technology demonstration instrument, and not an operational land imager, only one quarter of the ETM+ swath width is covered by an ALI acquisition (~37 km) (Ungar *et al.* 2003). However, the EO-1 satellite may be rolled to point to a specific location to achieve coverage anywhere in the Landsat swath.

The primary characteristics of the ALI reflective bands are listed in table 2 and contrasted with the Landsat ETM+ reflective bands. ALI does not have a thermal band, so Landsat ETM+ thermal data were not utilized in this study. Compared to ETM+, the ALI sensor has increased dynamic range (12 bit vs. 8 bit), improved signal-to-noise ratio (four to 10 times relative SNR, depending on the band

Table 2. Comparison of Landsat ETM+ and ALI spectral information.

Landsat ETM+ 30 m bands	ETM+ wavelength (nm)	ALI 30 m bands	ALI wavelength (nm)
		1p	432–451
1	450–520	1	458–511
2	530–610	2	532–602
3	630–690	3	632–688
4	780–900	4	775–805
		4p	844–888
		5p	1200–1288
5	1550–1750	5	1554–1725
7	2090–2350	7	2090–2362

(Mendenhall *et al*. 2002)), and additional bands in the blue (442 nm), the near-infrared (866 nm), and the short-wave infrared (1244 nm) portions of the spectrum. The EO-1 mission was originally planned to be 1 year in duration; however, the satellite continues to be operational. A series of eight ALI scenes spanning the 2001 and 2002 Okavango flooding season was acquired by NASA for the EO-1 calibration/validation program. Five cloud-free ALI scenes (31 May, 16 June, 11 July, and 19 August 2001 and 16 September 2002) were analysed in this study. The ALI data acquired in 2001 and 2002 provide the best temporal sequence obtained to date for mapping and monitoring the Okavango Delta. Fortunately, near cloud-free conditions occur continuously during the flooding season, thereby resulting in excellent quality imagery.

3.2 *Data pre-processing*

Because the ALI sensor is a technology demonstration instrument, additional pre-processing of the Level 1R data product (relative to what is necessary for Landsat ETM+) is required prior to analysis (Goodenough *et al*. 2003). The two-dimensional arrays of detectors on ALI populate four Sensor Chip Assemblies (SCAs) (figure 2), thereby resulting in four strips of data that must be radiometrically balanced and mosaicked. The physical offset of the bands on each SCA necessitates alignment of bands, as well as of SCAs. Striping in data acquired by pushbroom sensors is typically caused by inter-detector variations in calibration,

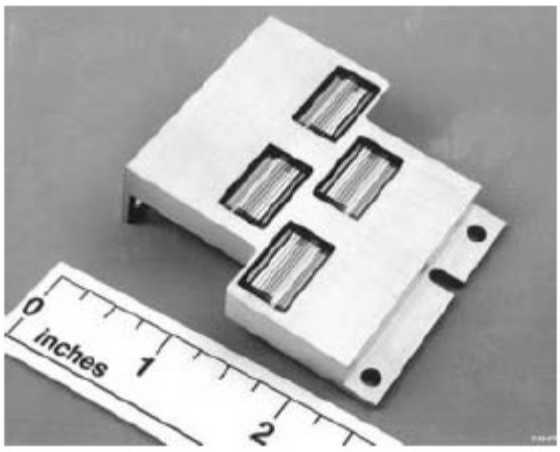

Figure 2. ALI sensor chip assembly (SCA) (from Ungar *et al*. 2003).

failed or 'bad' detectors, transient environmental conditions, or internal system anomalies. Depending on the source of the striping, a partial or complete column is affected and is either totally unusable or requires normalization. Failed or 'bad' detectors result in a full column of null data at their respective position in the array. Once identified, their effect can be corrected readily as they occur in all data. In this study, data in columns (j) associated with bad detectors were removed and replaced by the average of the adjacent ($j \pm 1$) columns in the same row.

Intermittently and partially streaked columns are associated with transient phenomena and can often be detected and normalized to produce usable data. Columns containing these data were detected in each scene using a two-step process. First, the difference between sample means of data from adjacent columns was compared to a threshold to identify candidate columns containing 'problematic' data. Individual pixels within these candidate columns were flagged if their digital number (DN) value was sufficiently different from that of the immediate ($j \pm 1$) and ($j \pm 2$) neighbours. Groups of at least n (user specified) consecutive pixels within a column were considered as streaks and assigned to an associated streaked subset (Goodenough *et al.* 2003). The streaked subsets were then 'corrected' by normalizing columns such that their means and variances matched those of a local moving window centred over the column, as shown in figure 3. For this study, six consecutive pixels were flagged as a streak and corrected with a local window of size 10×5 pixels (Neuenschwander 2003). In addition to detector corrections within individual strips, calibration-based differences between the four SCAs must be normalized. An empirical correction to match the mean of the 10 pixel overlap region between successive SCAs was applied to SCAs 1–3, assuming that SCA4 was relative 'truth'.

A simple full pixel shift to provide approximate band-to-band co-location is provided in the Level 1R product, but was not considered adequate for analysis of this landscape where features change within tens of metres. Further, adjustments are scene-dependent because the satellite can be pointed to image a specified target. A

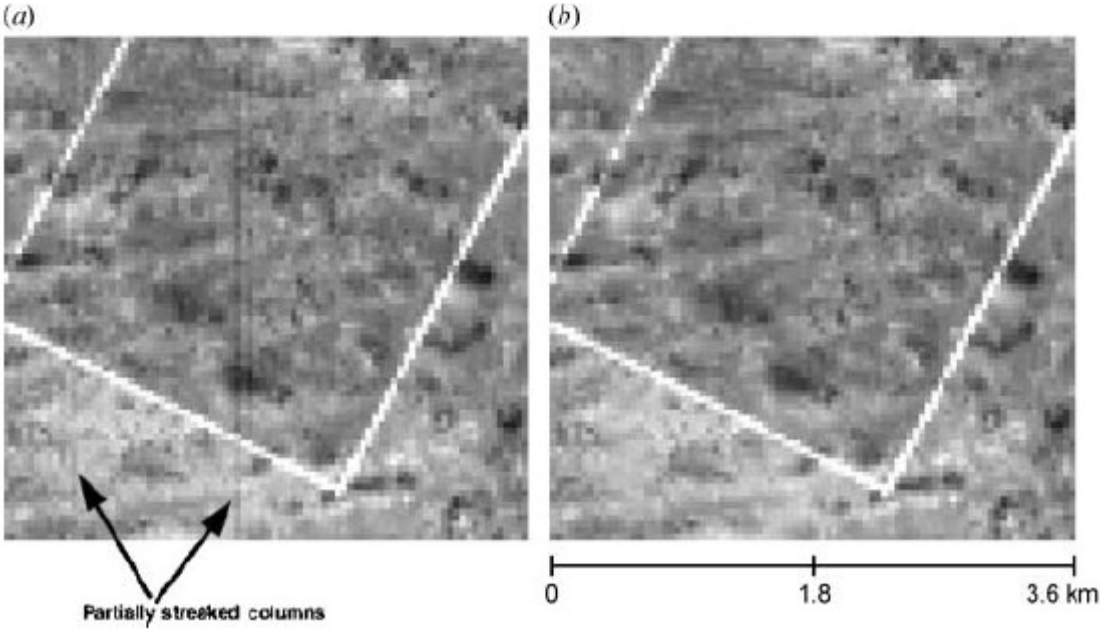

Figure 3. Example of ALI band 7 (*a*) partially streaked columns due to inter detector calibration problems and (*b*) after correction.

standard pre-launch line of sight map (LOS) surveying the locations of the individual detectors on the array was developed to map the energy received on the focal plane to each detector. A method which incorporates updated LOS maps for the detectors that was later developed by MIT Lincoln Labs and the USGS EROS Data Center (EDC), was used here to align and mosaic the ALI data (Meyer *et al.* 2001, Storey *et al.* 2004). Map-oriented data were then obtained by combining LOS maps with the GPS and altitude information of the satellite. The final georeferencing was achieved by simple translation of the resultant image to match a Landsat ETM+ basemap scene. All scenes were georeferenced to a UTM 34 S projection with a WGS84 ellipsoid. Both ALI and ETM+ data were corrected for sun angle but were not atmospherically corrected prior to supervised classification of each image.

3.3 *Classification methodology*

The Bayesian Pairwise Classifier with Feature Selection (BPC-FS) method was utilized to classify the ALI and Landsat ETM+ data. The supervised method, which is fully described in Crawford *et al.* (1999), utilizes a class-dependent band selection technique in conjunction with a Bayesian pairwise classifier framework. The method decomposes a multiclass problem with $C(>2)$ classes into a set of $\binom{C}{2}$ simpler two-class problems. For each pair (i, j) of classes $(1 \leqslant i < j \leqslant C)$, a separate classifier is trained to distinguish between those classes. The method sequentially selects the most relevant bands to distinguish between each pair of classes based on their incremental contribution to either a log-odds relevance function or to classification accuracy, stopping when the relative change associated with the most recently selected band is less than a user-selected value. Each observation is labelled using every pairwise classifier. The ultimate class label for each observation is then selected either via voting or by the maximum Bayesian posterior probability rule applied to the posterior probabilities of the individual pairwise classifiers. The approach not only simplifies the original problem and potentially improves discrimination capability between pairs of classes with overlapping distributions, but also provides the flexibility of using any type of classifier and any band or combinations of bands to classify each class pair (i, j). The BPC-FS method typically yields classification accuracies that are higher than the traditional maximum-likelihood classifier, which labels each pixel as 1 of C classes in a single step, as it is better able to tune the bands and decision boundaries to each class pair. It also provides useful domain information on the required number and value of band combinations for discriminating between classes. This aspect of the classifier facilitated comparison of the results obtained using ALI and ETM+ data, as well as evaluation of the relative contribution of the additional ALI bands.

4. Results

4.1 *Land cover classification*

The four ALI data sets from 2001 (31 May, 16 June, 11 July, and 19 August) and a single ETM+ scene (12 August 2001) were first classified as members of the 23 land cover classes found in the seasonal and occasional swamps and drier woodlands listed in table 1. Training data were selected manually using a combination of GPS located vegetation surveys, aerial photography from the Aquarap (2000) project,

and 2.6 m resolution IKONOS multispectral imagery. Data sets were randomly sampled such that 50% of the data points were used for training, and 50% were reserved for testing the classifier. In order to compensate for bias associated with co-location of training and test data within patches, additional sites were selected and used for an independent determination of accuracies. These accuracies, which are lower than those of the training and test data, are reported in this paper. It was necessary to select training/test data from each ALI acquisition, since vegetation exhibited some seasonal spectral variation, and land cover conditions changed due to the progression of the flood front and burning that occurred between acquisitions. However, where possible, the training data were selected from the same geographic locations for the entire sequence of imagery.

Overall classification accuracies listed in table 3 are consistent for all 23 land cover classes spanning the four ALI data sets. The producer and user accuracies for each class are also detailed in table 3. Figure 4 shows the resulting land cover classification map obtained from classifying the 2001 ALI sequence using the BPC-FS method with all the ALI bands (1p-7) as candidate inputs. The lower accuracy for the 31 May data resulted from the poor discrimination of the acacia grasslands (class 9), where the majority of pixels were misclassified as dry grasses (class 12). The ETM+ data were also classified using the BPC-FS method. Most notable are the higher overall classification accuracies for the ALI data (~80%) compared to those of the 12 August ETM+ data (~68%) shown in table 4. This increase is attributed to both the higher signal-to-noise ratio and the increased dynamic range of the ALI data. Visual evaluation of the ETM+ classification output shows that the secondary flood plain (flood plain3—class 19) was often misclassified as interior island grasses (class 13). Also, the backswamp class (class 16) was often confused with water, causing the total flood extent to be overestimated.

As stated previously, the ALI sensor has three additional reflective bands relative to ETM+. ALI band 1p (442 nm, blue) was added for water quality applications. ETM+ band 4 was divided into two bands, ALI band 4 and ALI band 4p, to avoid the water absorption feature centred at 825 nm. ALI band 5p (1244 nm, shortwave infrared) was added to potentially improve discrimination of land cover. Of particular interest to the study was evaluation of the contribution of these additional bands to land cover mapping in the Delta. The BPC-FS provides some capability to determine the relative contribution of a band to a pairwise classifier in terms of whether a band is selected and the order in which it is selected. In multiple runs of the BPC-FS per scene, the band selection proved to be quite stable, with nearly the same bands selected for each class pair in most runs. The total number of bands selected for a representative single run is listed in table 5, and the number of times a band was selected as the first band, is listed in table 6. The bands selected for the 19 August ALI and the 12 August ETM+ data are listed in table 6 for comparison. The band selection ratio listed in tables 5 and 7, which is computed as the ratio of the total number of bands selected to the total number of class pairs, provides a simple indicator of the typical number of bands selected for classification of a given data set. The total number of times a band is selected, as well as the number of times a band is selected first, is an indication of the importance of that particular band for class discrimination. A lower band ratio would indicate that fewer bands were required to discriminate the same class pairs. The band ratio for the August ALI scene was 1.66, whereas the August ETM+ band ratio was 1.91. The BPC-FS typically required only

Table 3. Classification accuracies for 2001 ALI scenes.

Class	31 May ALI		16 June ALI		11 July ALI		19 August ALI	
	Producer accuracies	User accuracies	Producer accuracies	User accuracies	Producer accuracies	User accuracies	Producer accuracies	User accuracies
North riparian	74.32	51.64	67.92	55.10	57.80	64.10	69.86	55.30
South riparian	79.19	89.14	74.4	78.12	87.16	91.79	81.35	84.41
Mopane shrublands	86.44	96.23	88.55	79.89	71.37	94.74	66.51	94.70
Mopane woodlands	84.85	42.64	62.22	70.89	60.34	77.72	82.55	100.00
Acacia woodlands	90.43	87.18	90.54	92.41	100.00	89.53	100.00	95.97
Woodland mix	96.67	85.93	92.02	84.27	86.90	92.65	90.00	99.00
Acacia woodlands on CI	49.12	70.59	52.82	61.98	83.22	57.21	49.67	33.94
Acacia shrublands on CI	37.70	30.40	66.88	46.32	70.16	75.00	42.31	56.20
Acacia grasslands on CI	17.24	37.04	85.25	77.61	84.28	92.41	85.71	71.43
Mopane/pechuel/grass mix	95.92	87.04	72.88	68.25	91.48	64.14	97.95	72.22
Grass/pechuel mix	97.28	96.62	88.17	96.13	90.66	86.84	98.71	89.47
Dry grasses	68.57	38.87	69.54	76.09	52.94	61.54	59.06	55.00
Island interior	84.50	98.83	75.66	95.04	53.85	76.36	58.74	87.33
Exposed soil	84.68	69.54	93.88	76.24	94.97	69.59	80.60	77.59
Reeds	97.08	95.95	88.62	96.10	99.43	96.65	90.91	94.94
Backswamp	91.59	90.39	85.44	85.44	73.10	93.81	64.34	97.65
Floodplain grasses 1	35.37	87.88	78.66	87.16	72.67	64.77	96.95	71.75
Floodplain grasses 2	80.65	95.24	64.48	94.40	80.32	98.69	87.05	85.71
Floodplain grasses 3	39.02	51.61	80.93	65.69	76.35	56.36	73.14	65.31
Water	91.28	97.27	90.43	100.00	99.55	100.00	100.00	100.00
Aquatic vegetation	83.97	93.22	96.20	86.86	94.08	100.00	94.79	99.45
Firescar1	53.95	100.00	78.00	97.50	N/A	N/A	100.00	98.92
Firescar2	97.53	69.00	84.51	90.91	82.63	88.20	98.31	98.31
Overall	74.90%		79.60%		80.30%		80.80%	
Kappa	0.7373		0.7871		0.7933		0.7984	

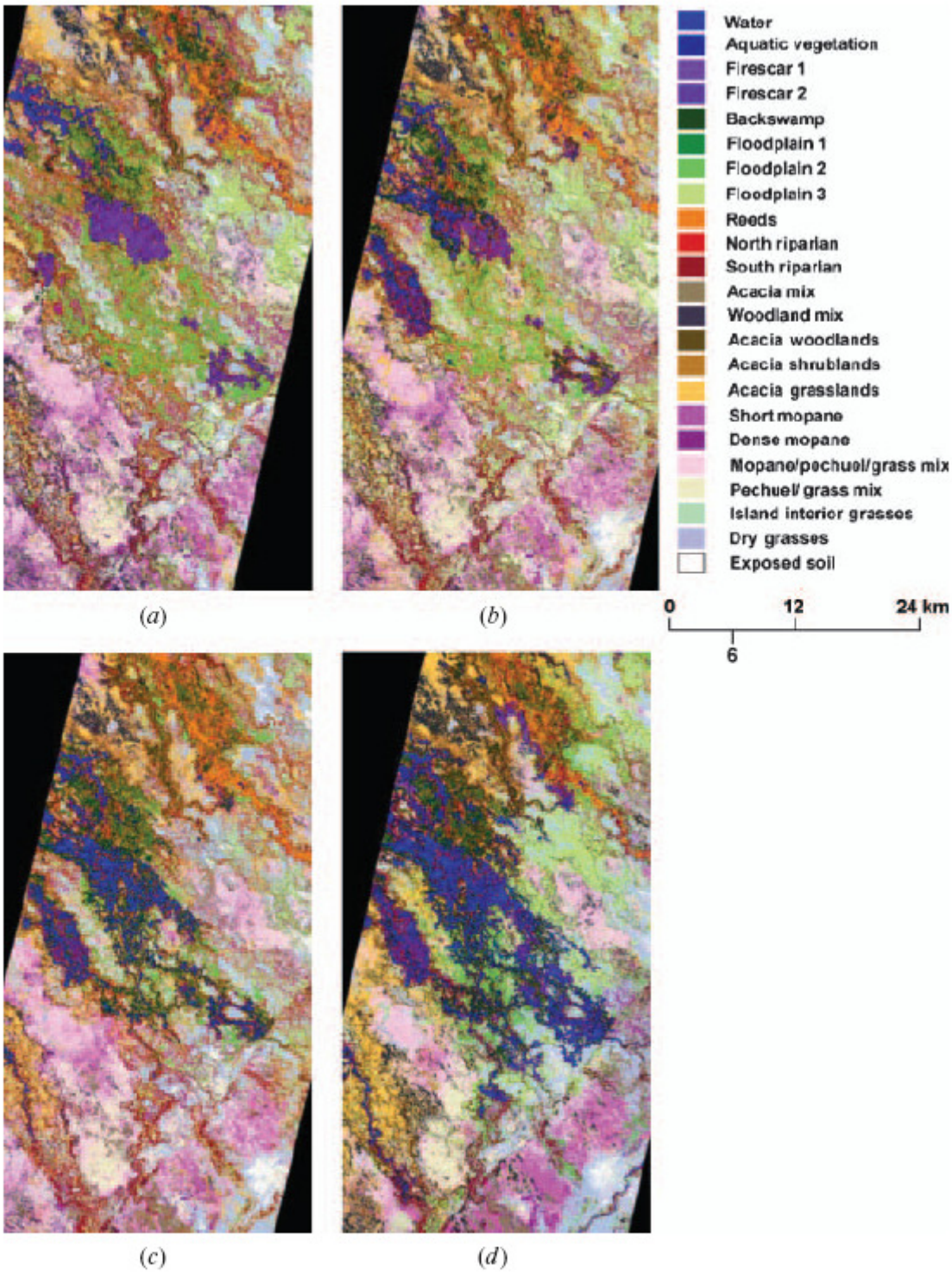

Figure 4. Classification of 2001 ALI data over study area using BPC-FS algorithm for (*a*) 31 May, (*b*) 16 June, (*c*) 11 July, and (*d*) 19 August.

one or two bands to distinguish between each class pair for ALI, as shown in table 5. Band 5p was selected more frequently than band 5 and was more often the first band chosen as there was greater separation of class signatures in these scenes in ALI band 5p than in ALI band 5. Bands 1 and 2 (480 nm and 567 nm, blue and green portion of the spectrum) were selected least frequently. However, they were typically the dominant band for discriminating tree dominated classes. Despite its

Table 4. Classification accuracies for ETM+ (12 August) and ALI (19 August).

	19 August 2001 ALI		12 August 2001 ETM+	
Class	Producer accuracies	User accuracies	Producer accuracies	User accuracies
North riparian	69.86	55.30	36.36	38.78
South riparian	81.35	84.41	64.25	59.62
Mopane shrublands	66.51	94.70	59.07	76.51
Mopane woodlands	82.55	100.00	59.64	62.84
Acacia woodlands	100.00	95.97	99.16	71.08
Woodland mix	90.00	99.00	71.82	81.44
Acacia woodlands on CI	49.67	33.94	49.67	29.76
Acacia shrublands on CI	42.31	56.20	34.07	43.36
Acacia grasslands on CI	85.71	71.43	65.71	56.44
Mopane/pechuel/grass mix	97.95	72.22	91.10	79.17
Grass/pechuel mix	98.71	89.47	91.61	84.52
Dry grasses	59.06	55.00	46.98	61.40
Island interior	58.74	87.33	30.04	44.37
Exposed soil	80.60	77.59	81.47	75.60
Reeds	90.91	94.94	79.39	80.86
Backswamp	64.34	97.65	64.34	85.57
Floodplain grasses 1	96.95	71.75	67.94	61.81
Floodplain grasses 2	87.05	85.71	72.54	62.22
Floodplain grasses 3	73.14	65.31	30.29	29.78
Water	100.00	100.00	99.63	99.26
Aquatic vegetation	94.79	99.45	95.83	98.92
Firescar1	100.00	98.92	96.74	98.89
Firescar2	98.31	98.31	96.61	95.00
Overall	80.80%		67.87%	
Kappa	0.7984		0.6634	

low signal-to-noise ratio, band 1p was selected in all ALI scenes. Additionally, it contributed to improved classification accuracies, especially for woodland dominated classes, as determined by experiments from which it was omitted.

4.2 *Flood mapping*

Investigation of the variability in annual flood patterns of the lower Okavango Delta was a primary science objective of the study. The Okavango experiences several months with no rainfall during the dry winter season, yet because of the

Table 5. Frequency of band selection by BPC-FS classifier for 2001 ALI experiments.

ALI band	31 May	16 June	11 July	19 August
1p	36	35	56	34
1	26	19	24	37
2	21	21	31	35
3	43	67	68	63
4	50	64	37	28
4p	35	40	37	49
5p	82	47	52	65
5	50	31	21	40
7	57	77	38	70
Total	400	401	364	421
Band ratio	1.588	1.58	1.57	1.66

Table 6. First bands selected by BPC-FS classifier for 2001 ALI experiments.

ALI band	31 May	16 June	11 July	19 August
1p	20	22	42	22
1	12	13	14	38
2	12	16	21	22
3	18	41	41	44
4	40	50	28	14
4p	25	21	26	32
5p	56	28	26	42
5	34	14	8	14
7	36	48	25	35

temporal lag of upstream rainwater, the Delta floods during this dry season. Thus, it is safely assumed that the surface water detected in this study is a result of seasonal flooding, and not localized precipitation. The progression of the 2001 flooding event in the study area is evident in the classification maps derived from the ALI data (figure 4). The variability in inter-annual flood patterns is clearly visible in figure 5, which depicts corresponding total flood cover in 2001 and 2002 derived from the ETM+ sensor. The total annual flood extent obtained from the ALI and ETM+ sensors was similar visually and in total area, as shown in table 8. Here, the total water area was determined as the product of the sensor resolution and the number of pixels classified as water. Similarly, the total inundated area was computed as the product of the sensor resolution and the sum of the pixels classified as water or backswamp. The ALI data used in this comparison were acquired on 19 August 2001 and 16 September 2002, and the ETM+ data were acquired on 12 August 2001 and 31 August 2002. Backswamp was often misclassified as water using ETM+ data, which in turn overestimated the amount of water present in the Delta. From the estimated flooding extent, it appears that the total quantity of water flowing into the study area was approximately the same in 2001 and 2002. The primary difference between the flooding for these two years was exhibited in the spatial distribution and flooding patterns. The amount of water derived from analysis of the ALI data is consistent from 2001 to 2002 (~124 km^2), but differs for the ETM+ data (~232 km^2 in 2001 and 156 km^2 in 2002), which is partially attributed to the misclassification of backswamp as water in the ETM+ data. The total inundated area (water and

Table 7. Frequency of total bands selected by BPC-FS for August 2001 ALI and ETM+ data.

ALI band	ALI 19 August	ETM+ band	ETM+ 12 August
1p	34		
1	37	1	43
2	35	2	56
3	63	3	91
4	28	4	137
4p	49		
5p	65		
5	40	5	68
7	70	7	88
Total	421		483
Band ratio	1.66		1.91

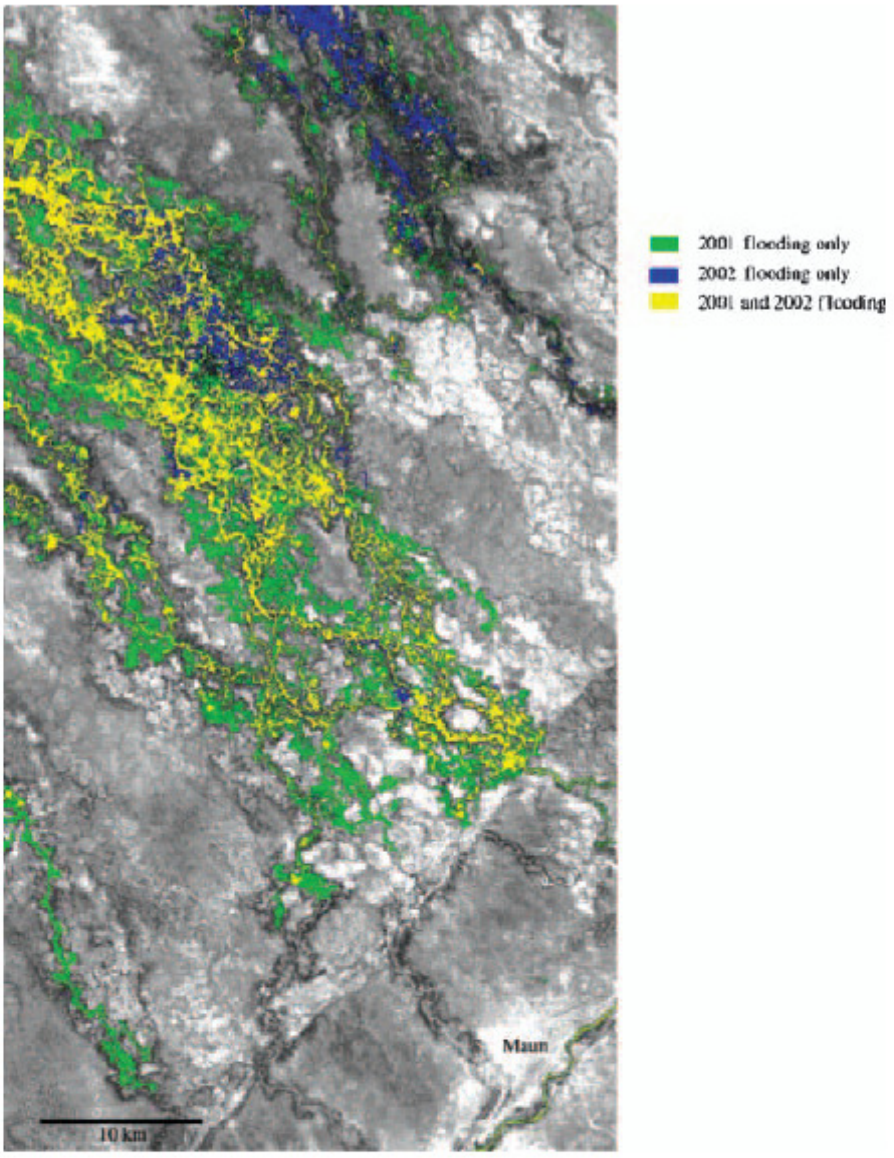

Figure 5. Total flood cover map derived from 12 August 2001 and 31 August 2001 Landsat ETM+ data for study area.

Table 8. Class areas for inter-annual flood map (km^2).

	Total water area (km^2)	Total inundated area [water and backswamp] (km^2)
ETM+ derived		
12 August 2001	232	257
31 August 2002	156	200
ALI derived		
19 August 2001	122	257
16 September 2002	124	158

backswamp combined) of ALI and ETM+ was 257 km^2 in 2001. The peak of the flooding usually occurs in mid-August, and water recedes from the backswamp first. This is likely the primary source of the differences in total water cover using ETM+ data from August 2001 and September 2002, respectively.

5. Discussion

While pre-processing the ALI data mitigated radiometric and geometric distortions, it may also have contributed to some classification errors. For example, varying pointing angles can result in slight misalignment of data within the overlap regions of the SCAs. The potential of misalignment can have a significant impact on land cover mapping in the Delta where some land cover classes (e.g. riparian and reeds) occupy narrow corridors. Similarly, the limitations of the radiometric adjustment procedure are acknowledged. However, classification accuracies obtained using the 'corrected' ALI data were superior to those obtained using ETM+ data. This is important as improvements in land cover classification can lead to improved estimates of land surface parameters, and thereby better understanding and modelling of land surface processes. In addition, accurate determination of land cover in the Delta is critical to understanding the impacts of disturbance regimes (e.g. flooding, fire, or grazing) on ecosystem functioning.

Reeds and sedges were difficult to discriminate in a previous classification of Landsat ETM+ data acquired over the Delta (Ringrose *et al.* in press a). In the current study, high classification accuracies were achieved for reeds (class 15), and better separation of the reeds and flood-plain vegetation from the riparian class, as measured by the accuracies from the pairwise classifier, occurred in ALI data than in Landsat ETM+ data. This improvement is critical, as the riparian vegetation is thought to be a significant factor in the evapotranspiration processes in the lower Delta. It is also noteworthy that ALI band 5p was always selected by classifiers involving the difficult reed and water classes. Discrimination of riparian vegetation actually improved in experiments where band 5 was excluded, whereas it was confused with floodplain and reeds when band 5 was included. As noted previously, the classifier also had difficulty separating water from backswamp using the ETM+ data as input. For these two class pairs, bands 7, 3, and 5 were selected by the classifier for ETM+ data, whereas bands 5 and 3 were selected using the ALI data. Overall, comparable spectral bands were selected for discriminating given pairs of classes in ETM+ data. For both ALI and ETM+, additional bands were required for problematic classes such as north riparian (class 1) and reeds (class 15). Further investigation of the discrimination of spectrally similar land cover types is planned with EO-1 Hyperion hyperspectral data, which are acquired concurrently on the same platform.

Spatial variability of the flooding patterns and its impact on biota of the Delta are not well understood, but are critical for management of the ecosystem. Although hydrologic models have been developed which model the inflow and outflow from the Delta, they have not focused on the spatial patterns of the seasonal flooding. While the aggregate quantity of annual rainfall upriver is important, much of the variability in flood patterns is associated with the shallow, anastomosing channels that comprise most of the Delta. In addition, information on the evapotranspiration process is essentially unknown for the tributaries within the Delta (Ringrose in press a). The inter-annual flooding differences observed in the

ALI imagery include the Marophe Channel, which did not flood in 2002, and the lower Boro River. The floodplains surrounding the Boro River were flooded more extensively in 2001, whereas in 2002, the water was confined to the primary channels. It is speculated that some of the differences in the inter-annual variability in spatial distribution of flood waters can be attributed to burning or other factors that affect the vegetation and impedance to the flow of water. This conjecture, however, cannot be tested until analysis on additional intra-annual data from 2002 and 2003 is completed.

6. Conclusions

This preliminary study in the use of EO-1 multispectral data, for both mapping land cover characteristics and studying phenomena related to annual flooding, indicates that the improved spectral characteristics of ALI data were useful. The superiority of EO-1 ALI data was manifested both in higher classification accuracies and in visual analysis of the multispectral imagery. The study also indicates that ALI band 5p, centred at the 1244 nm wavelength, was a valuable addition to the ALI instrument. It was often selected in the BPC-FS and provided better separation of land cover classes than ALI band 5. Because ETM+ band 4 was essentially divided into two bands for the ALI (band 4 and 4p), no significant improvements in classification were expected, since both bands could be selected by the BPC if their individual contributions were significant. The benefit of splitting ETM+ band 4 into two bands is the reduction in the contribution of the water absorption feature in ETM+ band 4.

The BPC-FS classification method utilized fewer bands that were highly correlated than a standard classification that typically uses all bands. This improves parameter estimates, particularly for pairs of classes with small amounts of training data. While this is not as critical for analysis of multispectral data, it is extremely important for classification of hyperspectral data. The second phase of this ongoing study involves analysis of Hyperion data acquired simultaneously to ALI on the EO-1 platform. The BPC-FS method provides a useful framework that can be used with various feature selection and extraction methods, which are required to reduce the dimensionality of the hyperspectral input. The pairwise approach also provides a foundation for knowledge transfer that will be investigated as the classifier is utilized beyond the area on which it was originally trained. Finally, the simpler individual classifiers utilized by the BPC-FS often provide insight into class-dependent physiological phenomena. This aspect is currently being studied in terms of the resultant class dependent features that were selected by the BPC-FS.

Acknowledgements

This research was supported in part by the National Aeronautics and Space Administration EO-1 program (NCC5-463) and the Army Research Office Terrestrial Sciences Program (DAAG55-98-1-0287). Landsat ETM+ and IKONOS data were provided through the NASA SAFARI 2000 Southern African Regional Science Initiative program. Additional logistical support was provided by the Harry Oppenheimer Okavango Research Center, Maun, Botswana. Acquisitions of both ALI and Hyperion, the hyperspectral sensor on EO-1, can be requested, and data can be obtained from the USGS EROS Data Center (EDC).

References

AQUARAP, 2000, Rapid Assessment of the Aquatic Ecosystems of the Okavango Delta (Unpublished CD-ROM). Conservation International, Botswana.

CRAWFORD, M.M., KUMAR, S., RICARD, M.R., GIBEAUT, J.C. and NEUENSCHWANDER, A.L., 1999, Fusion of airborne polarimetric and interferometric SAR data for classification of coastal environments. *IEEE Transactions on Geoscience and Remote Sensing*, **37**, pp. 1306–1315.

GOODENOUGH, D.G., DYK, A., NIEMANN, K.O., PEARLMAN, J.S., CHEN, H., HAN, T., MURDOCH, M. and WEST, C., 2003, Processing Hyperion and ALI for forest classification. *IEEE Transactions on Geoscience and Remote Sensing*, **41**, pp. 1321–1331.

KEDDY, P., 2000, *Wetland Ecology: principles and conservation* (Cambridge, UK: Cambridge University Press).

MCCARTHY, T.S. and ELLERY, W.N., 1993, The Okavango Delta. *Geobulletin*, **36**(2), pp. 5–8.

MCCARTHY, T.S., BARRY, M., BLOEM, A., ELLERY, W.N., HEISTER, H., MERRY, C.L., RUTHER, H. and STERNBERG, H., 1997, The gradient of the Okavango Fan, Botswana, and its sedimentological and tectonic implications. *Journal of African Earth Sciences*, **24**, pp. 65–78.

MCCARTHY, T.S., BLOEM, A. and LARKIN, P.A., 1998, Observations on the hydrology and geohydrology of the Okavango Delta. *South Africa Journal of Geology*, **101**, pp. 101–117.

MENDENHALL, J.A., LENCIONI, D.E. and EVANS, J.B., 2002, EO-1 Advanced Land Imager Technology Validation Report. EO-1-9, MIT/Lincoln Laboratory, USA.

MEYER, D., STOREY, J., CHOATE, M., MORFITT, R., HELDER, D. and RUGGLES, T., 2001, EO-1 Advanced Land Imager geometric characterization preliminary results. In *EO-1 Science Validation Meeting*, 1–4 May 2001, Tucson, AZ.

MLGLH (MINISTRY OF LOCAL GOVERNMENT, LANDS, AND HOUSING), 1989, *Ecological Zoning of Okavango Delta*, Internal Report, Botswana.

NEUENSCHWANDER, A., 2003, Characterization of the vegetation of the Okavango Delta, Botswana using EO-1 Data. Masters thesis, Department of Aerospace Engineering, University of Texas at Austin, United States.

RINGROSE, S., MATHESON, W. and BOYLE, T., 1988, Differentiation of ecological zones in the Okavango Delta, Botswana, by classification and contextual analysis of Landsat MSS data. *Photogrammetric Engineering and Remote Sensing*, **54**, pp. 325–332.

RINGROSE, S., VANDERPOST, C. and MATHESON, W., 1997, Use of image processing and GIS techniques to determine the extent and possible causes of land management/fenceline induced degradation problems in the Okavango area, northern Botswana. *International Journal of Remote Sensing*, **18**, pp. 2337–2364.

RINGROSE, S., MATHESON, W. and VANDERPOST, C., 2003, Mapping ecological conditions in the Okavango Delta, Botswana, using fine and coarse resolution systems including simulated SPOT VEGETATION imagery. *International Journal of Remote Sensing*, **24**, pp. 1029–1052.

RINGROSE, S., JELLEMA, A., HUNTSMAN-MAPILA, P., BAKER, L. and BRUBAKER, K., 2005, Use of remotely sensed data in the analysis of soil-vegetation changes along a drying gradient peripheral to the Okavango Delta, Botswana. *International Journal of Remote Sensing*, **26**, pp. 4293–4319.

RINGROSE, S., MATHESON, W., JELLEMA, A. and ASHWORTH, M., in press a, Techniques for assessing the use of near surface groundwater by riparian trees in the distal Okavango Delta, Botswana. *Applied Geography*.

RINGROSE, S., KAMPUNZU, A.B., VINK, B., MATHESON, W. and DOWNEY, W.S., in press b, Origin and paleo-environments of calcareous sediments in the Moshaweng dry valley, southeast Botswana. *Earth Surface Processes and Landforms*.

STOREY, J.C., CHOATE, M.J. and MEYER, D.J., 2004, A geometric performance assessment of the EO-1 Advanced Land Imager. *IEEE Transactions on Geoscience and Remote Sensing*, **42**, pp. 602–607.

UNGAR, S.G., PEARLMAN, J., MENDENHALL, J.A. and REUTER, D., 2003, Overview of the Earth Observing-1 (EO-1) Mission. *IEEE Transactions on Geoscience and Remote Sensing*, **41**, pp. 1149–1159.

WHITE, F., 1983, The vegetation of Africa, A descriptive memoir to accompany the UNESCO/AETFAT/UNSO vegetation map. In *Natural Resources Research*, 365 pp. (Paris: UNESCO).

WOLSKI, P., GUMBRICHT, T. and MCCARTHY, T.S., 2002, Assessing future change in the Okavango Delta: The use of a regression model of the maximum annual flood in a Monte Carlo Simulation. In *Proceedings to Environmental Monitoring of Tropical and Subtropical Wetlands Conference*, December 2002, Maun, Botswana.